Large scale pressure fluctuations and the Sunyaev-Zel'dovich effect

Asantha Cooray*
Department of Astronomy and Astrophysics, University of Chicago, Chicago, Illinois 60637
(Received 15 May 2000; published 9 October 2000)

The Sunyaev-Zel'dovich (SZ) effect associated with pressure fluctuations of the large scale structure gas distribution will be probed with current and upcoming wide-field small angular scale cosmic microwave background experiments. We study the generation of pressure fluctuations by baryons which are present in virialized dark matter halos, with overdensities $\gtrsim 200$ and by baryons present in overdensities $\lesssim 10$. For collapsed halos, assuming the gas distribution is in hydrostatic equilibrium with matter density distribution, we predict the pressure power spectrum and bispectrum associated with the large scale structure gas distribution by extending the dark matter halo approach which describes the density field in terms of correlations between and within halos. The projected pressure power spectrum allows a determination of the resulting SZ power spectrum due to virialized structures. The unshocked photoionized baryons present in smaller overdensities trace the Jeans-scale smoothed dark matter distribution. They provide a lower limit to the SZ effect due to large scale structure in the absence of massive collapsed halos. We extend our calculations to discuss higher order statistics, such as bispectrum and skewness in SZ data. The SZ-weak lensing cross correlation is suggested as a probe of correlations between dark matter and baryon density fields, while the probability distribution functions of peak statistics of SZ halos in wide field CMB data can be used as a probe of cosmology and non-Gaussian evolution of large scale pressure fluctuations.

PACS number(s): 98.80.Es, 95.85.Nv, 98.35.Ce, 98.70.Vc

I. INTRODUCTION

In recent years, increasing attention has been given to the physical properties of the intergalactic warm and hot plasma gas distribution associated with large scale structure and the possibility of its detection (e.g., [1]). It is now widely believed that at least $\sim 50\%$ of the present day baryons, when compared to the total baryon density through big bang nucleosynthesis, are present in this warm gas distribution and have remained undetected given its nature (e.g., [2]). Currently proposed methods for the detection of this gas include observations of the thermal diffuse x-ray emission (e.g., [3]), associated x-ray and UV absorption and emission lines (e.g., [4]) and the resulting Sunyaev-Zel'dovich (SZ, [5]) effect (e.g., [6]).

The SZ effect arises from the inverse-Compton scattering of cosmic microwave background (CMB) photons by hot electrons along the line of sight. This effect has now been directly imaged towards massive galaxy clusters (e.g., [7,8]), where temperature of the scattering medium can reach as high as 10 keV, producing temperature changes in the CMB of order 1 mK at Rayleigh-Jeans wavelengths. Previous analytical predictions of the resulting SZ effect due to large scale structure have been based on either a Press-Schechter (PS [9]) description of the contributing galaxy clusters (e.g., [10,11]) or using a biased description of the pressure power spectrum with respect to the dark matter density field (e.g., [6]). Numerical simulations (e.g., [12–14]) are beginning to improve some of these analytical predictions, but are still limited to a handful of simulations with limited dynamical range and resolution. Therefore, it is important that one consider improving analytical models of the large scale structure SZ effect, and provide predictions which can be easily tested through simulations.

Our present study on the large scale baryon pressure and the resulting SZ effect is timely for several reasons, including the fact that improving numerical simulations have recently begun to make detailed predictions for the pressure power spectrum and SZ effect such that those predictions can be extended and improved with analytical models [12–14]. Also, several studies have considered the possibility that the large scale baryon distribution can be probed with upcoming CMB missions using the SZ effect (e.g., [6]). Our calculations can be used to further refine these predictions and to investigate the possibility how such analytical model as the one presented here can be tested with observations.

As part of this study, we extend previous studies by considering the full power spectrum and bispectrum, the Fourier space analog of the three-point function, of pressure fluctuations. The pressure power spectrum and bispectrum contain all necessary information on the large scale distribution of temperature weighted baryons, whereas the SZ power spectrum is only a projected measurement of the pressure power spectrum. This can be compared to weak gravitational lensing, where lensing is a direct probe of the projected dark matter density distribution. The bispectrum of pressure fluctuations, and SZ bispectrum, contain all the information present at the three-point level, whereas conventional statistics, such as skewness, do not. A useful advantage of using the 3D statistics, such as the pressure power spectrum, is that they can directly be compared to numerical simulations, while only 2D statistics, such as the projected pressure power spectrum along the line of sight, basically the SZ power spectrum, can be observed. Our approach here is to consider both such that our calculations can eventually be compared to both simulations and observations.

The calculation of pressure power spectrum and bispec-

*Email address: asante@hyde.uchicago.edu

trum requires detailed knowledge of the baryon distribution, which can eventually be obtained numerically through hydrodynamical simulations. Here, we provide an analytical technique to obtain the pressure power spectrum and bispectrum by describing the baryon distribution in the universe as (1) present in virialized halos with overdensities $\gtrsim 200$ with respect to background densities, (2) unshocked diffuse baryons in overdensities $\lesssim 10$ that trace a Jeans-smoothed dark matter density field, and (3) the intermediate overdensity region, which is likely to be currently undergoing in shock heating and falling on to structures such as filaments. In the present paper we discuss the first two regimes, while a useful approach to include the latter, through simulations, is discussed.

Our description of baryons present in virialized halos follows recent studies on the dark matter density field through halo contributions [15–17] following [18] and applied to lensing statistics in [19] and [20]. For the description of baryons, the critical ingredients are the PS formalism [9] for the mass function; the Navarro-Frenk-White (NFW) profile of [21], and the halo bias model of [22]. The baryons are assumed to be in hydrostatic equilibrium with respect to dark matter distribution, which is a valid assumption, at least for the high mass halos that have been observed with x-ray instruments, given the existence of regularity relations between cluster baryon and dark matter physical properties (e.g., [23]). We take two descriptions of the temperature structure: (1) virial temperature and (2) virial temperature plus an additional source of minimum energy. The latter consideration allows the possibility for a secondary source of energy for baryons, such as due to preheating through stellar formation and feedback processes. Numerical simulations (e.g., [1,24]), as well observations (e.g., [25,26]), suggest the existence of such an energy source. The low photoionized overdensity baryons are described following the analytical description of [27]. The fraction of baryons present in such low overdensities are assumed to follow what has been measured in numerical simulations of [1]. We suggest that such baryons provide a lower limit to the SZ effect in the absence of any contribution from baryons present in virialized halos.

Throughout this paper, we will take the cold dark matter model with a cosmological constant (ΛCDM) as our fiducial cosmology with parameters $\Omega_c = 0.30$ for the CDM density, $\Omega_b = 0.05$ for the baryon density, $\Omega_\Lambda = 0.65$ for the cosmological constant, $h = 0.65$ for the dimensionless Hubble constant and a scale invariant spectrum of primordial fluctuations, normalized to galaxy cluster abundances ($\sigma_8 = 0.9$; see [28]) and consistent with the Cosmic Background Explorer (COBE) [29]. For the linear power spectrum, we take the fitting formula for the transfer function given in [30].

The paper is organized as following: In Sec. II, we review the dark matter halo approach to modeling the density field and extend it to model properties associated with large scale baryon distribution, mainly the pressure fluctuations that contributes to the observable SZ effect. We suggest recent papers by Seljak [15], Ma and Fry [16], Cooray and Hu [20], and Scoccimarro *et al.* [17] for details on the dark matter halo approach and applications to other observable statistics such as galaxy properties and weak gravitational lensing. As necessary, we use techniques developed in these papers for our current calculation. In Sec. III we apply the formalism to the convergence power spectrum, skewness, and bispectrum. We conclude in Sec. IV with a summary of our main results.

II. DENSITY AND PRESSURE POWER SPECTRA

A. General definitions

In order to calculate the contribution to temperature anisotropies through SZ effect associated with large scale structure, we divide the LSS with overdensities $\gtrsim 200$ as collapsed and virialized halos with a gas distribution following hydrostatic equilibrium and with virial temperatures. The pressure power spectrum can be calculated using an extension to the dark matter halo approach by assuming a physical relation between baryons and dark matter.

The baryons with overdensities $\lesssim 10$ track the dark matter distribution and their power spectrum has been studied by [27]. These baryons have temperatures similar to photoionization energies of hydrogen and helium. Current numerical simulations, e.g., [1], suggest that most of the baryons are in such low overdensities at $z > 1$, while at present day, are in virialized halos. The calculation of the SZ effect due to such baryons follow [6], except that we include the redshift dependence of mass fraction within such low density halos following the numerical results of [1], and modify the mean temperature of such baryons to be consistent with photoionization energies.

First we discuss the pressure and related power spectra due to collapsed halos.

The dark matter profile of collapsed halos are taken to be the NFW [21] with a density distribution

$$\rho_\delta(r) = \frac{\rho_s}{(r/r_s)(1+r/r_s)^2}. \tag{1}$$

The density profile can be integrated and related to the total dark matter mass of the halo within r_v:

$$M_\delta = 4\pi\rho_s r_s^3 \left[\log(1+c) - \frac{c}{1+c}\right] \tag{2}$$

where the concentration, c, is r_v/r_s. Choosing r_v as the virial radius of the halo, spherical collapse tells us that $M = 4\pi r_v^3 \Delta(z)\rho_b/3$, where $\Delta(z)$ is the overdensity of collapse (see e.g., [31]) and ρ_b is the background matter density today. We use comoving coordinates throughout. By equating these two expressions, one can eliminate ρ_s and describe the halo by its mass M and concentration c.

Following [19], we take the concentration of dark matter halos to be

$$c(M,z) = a(z)\left[\frac{M}{M_*(z)}\right]^{-b(z)}, \tag{3}$$

where $a(z) = 10.3(1+z)^{-0.3}$ and $b(z) = 0.24(1+z)^{-0.3}$. Here $M_*(z)$ is the nonlinear mass scale at which the peak-height threshold, $\nu(M,z) = 1$. The above concentration is chosen so that dark matter halos provide a reasonable match

to the nonlinear density power spectrum as predicted by [32]; it extends the treatment of [15] to the redshifts of interest for the SZ effect. We caution the reader that Eq. (3) is only a good fit for the ΛCDM model assumed.

The gas density profile, $\rho_g(r)$, is calculated assuming the hydrostatic equilibrium between the gas distribution and the dark matter density field within a halo. This is a valid assumption given that current observations of halos, mainly galaxy clusters, suggest the existence of regularity relations, such as size-temperature (e.g., [23]), between physical properties of dark matter and baryon distributions.

The hydrostatic equilibrium implies

$$\frac{kT_e}{\mu m_p}\frac{d\log\rho_g}{dr} = -\frac{GM_\delta(r)}{r^2}, \tag{4}$$

where now the $M_\delta(r)$ is the mass only out to a radius of r. Note that we have assumed here an isothermal temperature for the gas distribution. Solving for the the equations above, we can analytically calculate the baryon density profile $\rho_g(r)$,

$$\rho_g(r) = \rho_{g0} e^{-b}\left(1+\frac{r}{r_s}\right)^{br_s/r}, \tag{5}$$

where b is a constant, for a given mass,

$$b = \frac{4\pi G\mu m_p \rho_s r_s^3}{k_B T_e}, \tag{6}$$

with the Boltzmann constant, k_B.

In general, the halos are described with virial temperatures

$$k_B T_e = \frac{\gamma G\mu m_p M_\delta(r_v)}{3r_v}, \tag{7}$$

with $\gamma = 3/2$ and $\mu = 0.59$. In addition, we also consider the possibility for the existence of a constant nongravitational energy in small mass halos, consistent with observations of galaxy groups, due to what is commonly known as ''preheating.'' The possibility for such a minimum energy for baryons today comes from heating before virialization due to energy injection and feedback processes such as processes associated with stellar formation. The total gas mass present in a dark matter halo within r_v is

$$M_g(r_v) = 4\pi\rho_{g0} e^{-b} r_s^3 \int_0^c dx\, x^2 (1+x)^{b/x}. \tag{8}$$

The physical properties of the profile defined in Eq. (5) for baryons within dark matter halos, and a comparison to commonly used profiles such as isothermal and so-called beta-profiles, can be found in [33] and [34]. Compared to conventional profiles, this profile has the advantage that it is directly related to the dark matter profile parameters, such as central density ρ_s and concentration via scale radius r_s, thus, any changes to the dark matter distribution produces resulting changes in the baryon distribution. Also, one can study the effect of temperature variations on the gas distribution as the parameter b defined in Eq. (6) depends on it. A proper normalization for the dark matter halo distribution containing baryons comes through the $c(M,z)$ relation in Eq. (3) such that the non-linear dark matter power spectrum is produced in numerical simulations by the same halos. Note that our hydrostatic equilibrium ignores the self-gravity contribution from baryons to the total potential as we only include the dark matter contribution to total mass. Since the baryon mass is expected to be $\lesssim 10\%$ of the total mass, we can safely ignore, as a first approximation, the contribution to total mass from baryons themselves.

Roughly speaking, the perturbative aspect of the clustering of the dark matter and baryons is described by the correlations between halos, whereas the nonlinear aspect is described by the correlations within halos, i.e., the halo profiles. We will consider the Fourier analogies of the two and three point correlations of the dark matter density, δ, baryon pressure, Π, and galaxy distribution, g, defined in the usual way

$$\langle \delta_i^*(\mathbf{k})\,\delta_i(\mathbf{k}')\rangle = (2\pi)^3\delta(\mathbf{k}-\mathbf{k}')P_i^{\rm t}(k), \tag{9}$$

$$\langle \delta_i(\mathbf{k}_1)\,\delta_i(\mathbf{k}_2)\,\delta_i(\mathbf{k}_3)\rangle = (2\pi)^3\delta(\mathbf{k}_1+\mathbf{k}_2+\mathbf{k}_3) \times B_i^{\rm t}(k_1,k_2,k_3), \tag{10}$$

with i representing δ, Π or g. We will also consider cross-correlations between the two, such as the dark matter density-pressure power spectrum $P_{\delta\Pi}^{\rm t}(k)$, which is what one probes by correlating, say, the SZ effect and weak gravitational lensing observations. Here and throughout, we occasionally suppress the redshift dependence where no confusion will arise.

As presented in [20], these spectra are related to the *linear* density power spectrum $P(k)$ through the bias parameters and the normalized 3D Fourier transform of the density profile $\rho_i(r,M)$:

$$y_i(k,M) = \frac{1}{M_i}\int_0^{r_v} dr\, 4\pi r^2 \rho_i(r,M)\frac{\sin(kr)}{kr}, \tag{11}$$

where i represents either the density, δ, or the gas, g, profile and associated masses respectively given in Eqs. (2) and (8). With an increase in temperature relative to the virial temperature of the halo, especially for halos with masses $\lesssim 10^{13}\,M_\odot$, the gas profile is such that it does not fall rapidly at the virial radius, leading to an arbitrary cutoff when doing the Fourier transformation. We included an additional filter to the gas density profile such that the gas density profile decreases smoothly but promptly to zero at the virial radius: $\rho'(r) = \rho(r)[\mathrm{erfc}(r-r_v/\sqrt{2}\Delta r)-1]$ with $\Delta r \lesssim r_s$. Detailed aspects of the pressure and SZ statistics due to medium to small mass halos ($\lesssim 10^{13}\,M_\odot$) are sensitive to sharpness of this transition, but these issues do not change our primary results. Here, we concentrate mostly on the statistics due to massive and rare halos. Another possibility not considered here is to include the role of baryons at the outskirts of halos. The physical properties of such baryons can

be semianalytically calculated following the assumption that virial radius provides a shock boundary for the equilibrium of baryons within and outside virialized regimes. The baryons outside halos are likely to be preheated and trace the Jeans-smoothed version of the dark matter density field. The proper inclusion of such baryons requires the aid of numerical simulations or semianalytical models. These baryons are likely to include the ones present in overdensities between 200 and 10, which we have neglected in the present calculation.

Following [20], it is convenient to define a general integral over the halo mass function dn/dM,

$$I^{\beta,\eta,\gamma}_{\mu,i_1\ldots i_\mu}(k_1,\ldots,k_\mu;z)\equiv\int dM\left(\frac{M}{\rho_b}\right)^{\mu}\frac{dn}{dM}(M,z)b_\beta(M)\left(\frac{\rho_b}{M}\frac{\langle N_g\rangle}{\overline{n_g}}\right)^{\gamma}\times T_e(M,z)^{\eta}y_{i_1}(k_1,M)\ldots y_{i_\mu}(k_\mu,M), \tag{12}$$

where $b_0\equiv 1$ [22] gives the following analytic predictions for the bias parameters which agree well with simulations:

$$b_1(M;z)=1+\frac{\nu^2(M;z)-1}{\delta_c}, \tag{13}$$

and

$$b_2(M;z)=\frac{8}{21}[b_1(M;z)-1]+\frac{\nu^2(M;z)-3}{\sigma^2(M;z)}. \tag{14}$$

Here, $T_e(M,z)$ is the electron temperature of the baryon distribution of a given halo when pressure power spectrum is considered, $\nu(M,z)=\delta_c/\sigma(M,z)$, where $\sigma(M,z)$ is the rms fluctuation within a top-hat filter at the virial radius corresponding to mass M, and δ_c is the threshold overdensity of spherical collapse (see [31] for useful fitting functions).

The terms related to the galaxy power spectrum includes the average number of galaxies per dark matter halo, $\langle N_g\rangle$, the mean number density of galaxies in the universe $\overline{n_g}$. These parameters are discussed in Sec. II E involving the galaxy-pressure power spectrum.

We use the Press-Schechter (PS; [9]) mass function to describe dn/dM. We take the minimum mass to be 10^3 $M_\odot$ while the maximum mass is varied to study the effect of massive halos on related statistics. In general, masses above 10^{16} $M_\odot$ do not contribute to low order statistics due to the exponential decrease in the number density of such massive halos.

To summarize, in comparison to previous work on the SZ effect from virialized halos, our model has following advantages: (1) a physically motivated profile for the distribution of baryons in virialized dark matter halos, instead of an assumed profile such as the isothermal model or so-called β-profile; (2) a mass function for the virialized structures with the dark matter distribution of such halos reproducing the numerically simulated dark matter power spectrum and higher order correlations; (3) easily extendable variations to the baryon physics so as to account for issues such as preheating; (4) direct calculation of 3D properties of the large scale baryon distribution, such as the pressure power spectrum and bispectrum, which can be compared easily in numerical simulations.

We now discuss the calculation of properties related to the dark matter and baryons. In the case of baryons, we discuss pressure as this is the property that leads to the SZ effect allowing a useful probe of them.

B. Density power spectrum

Following [15], we can decompose the density power spectrum, as a function of redshift, into contributions from single halos (shot noise or ''Poisson'' contributions),

$$P^{\rm PP}_{\delta\delta}(k)=I^{0,0,0}_{2,\delta\delta}(k,k), \tag{15}$$

and correlations between two halos,

$$P^{\rm hh}_{\delta\delta}(k)=[I^{1,0,0}_{1\delta}(k)]^2P(k), \tag{16}$$

such that

$$P^{\rm t}_{\delta\delta}=P^{\rm PP}_{\delta\delta}+P^{\rm hh}_{\delta\delta}. \tag{17}$$

As $k\to 0$, $P^{\rm hh}_{\delta\delta}\to P(k)$.

C. Pressure power spectrum

As above, we can decompose the pressure power spectrum, as relevant for the SZ effect, into contributions from single halos

$$P^{PP}_{\Pi\Pi}(k)=I^{0,2,0}_{2,gg}(k,k), \tag{18}$$

and correlations between halos

$$P^{hh}_{\Pi\Pi}(k)=[I^{1,1,0}_{1,g}(k)]^2P(k), \tag{19}$$

such that

$$P_{\Pi\Pi}(k)^{\rm t}=P^{PP}_{\Pi\Pi}(k)+P^{hh}_{\Pi\Pi}(k). \tag{20}$$

For the pressure power spectrum, since η in Eq. (12) is nonzero, there is additional mass weighing arising from the fact that $T_e\propto M^{2/3}$ resulting in an additional mass dependence. The dependence is such that most of the contributions to the pressure, and thus, to the SZ, power spectrum come from most massive and rarest halos. This dependence has already been observed in numerical simulations by [14].

As we discuss later, this dependance on high mass halos to produce most of the pressure fluctuations also leads to several interesting results with regards to the detection and observability of SZ effect, among which are (1) most of the contribution to large scale SZ effect results from massive clusters of galaxies, while smaller mass halos and structures at low electron temperatures such as filaments do not contribute significantly, and (2) since massive halos dominate the SZ effect, and the distribution of these halos are Poisson and highly non-Gaussian, most of the contributions to two point and higher-order statistics of SZ effect will be domi-

nated by the Poisson term and there will be a significant non-Gaussianity associated with large scale SZ effect.

In fact, as we find later, the large scale correlations only contribute at a level of 10% to the SZ power spectrum suggesting that such correlations can be mostly disregarded. The non-Gaussianity associated with the SZ effect may become a useful tool to separate out its contribution from other sources of foregrounds in CMB anisotropy data, though this task can be efficiently carried out using frequency information (see [6]). We will return to all these issues in later sections.

D. Density-pressure power spectrum

The cross correlation between the density and gas field, as appropriate for lensing-SZ cross correlation can be decomposed as a single halo

$$P^{PP}_{\Pi\delta}(k)=I^{0,1,0}_{2,g\delta}(k,k), \tag{21}$$

and

$$P^{hh}_{\Pi\delta}(k)=[I^{1,1,0}_{1,g}(k)][I^{1,0,0}_{1,\delta}(k)]P(k), \tag{22}$$

such that

$$P_{\Pi\delta}(k)^{\rm t}=P^{PP}_{\Pi\delta}(k)+P^{hh}_{\Pi\delta}(k). \tag{23}$$

With the pressure and density field power spectra, one can define a bias associated with the large scale pressure, relative to density field,

$$b_\Pi(k)\overline{T_e}=\sqrt{\frac{P_\Pi(k)}{P_\delta(k)}}, \tag{24}$$

and the dimensionless correlation coefficient between the dark matter and baryon distributions

$$r_\Pi(k)=\frac{P_{\Pi\delta}(k)}{\sqrt{P_\delta(k)P_\Pi(k)}}. \tag{25}$$

In Eq. (24), the average density weighted temperature is

$$\overline{T_e}=\int dM\frac{M}{\rho_p}\frac{dn}{dM}(M,z)T_e(M,z). \tag{26}$$

Following [36], one can define a covariance matrix in Fourier space containing the full information on scale dependence of bias and correlations:

$$\hat{\mathbf{C}}(k)\equiv\begin{pmatrix}P_{\delta\delta}(k) & P_{\Pi\delta}(k)\\ P_{\Pi\delta}(k) & P_{\Pi\Pi}(k)\end{pmatrix}=P_{\delta\delta}(k)\begin{pmatrix}1 & b_\Pi r_\Pi\\ b_\Pi r_\Pi & b^2_\Pi\end{pmatrix}. \tag{27}$$

The observation measurement of b_Π and r_Π can be considered by an inversion of the SZ-SZ, lensing-lensing and SZ-lensing power spectra as a function of redshift bins in which lensing-lensing or SZ-lensing power spectra are constructed. We discuss these possibilities later.

E. Galaxy-pressure power spectrum

The cross correlation between the galaxy distribution and gas field, as appropriate for galaxy-SZ cross correlation can be decomposed as a single halo

$$P^{PP}_{\Pi\delta}(k)=I^{0,1,1}_{2,g\delta}(k,k), \tag{28}$$

and

$$P^{hh}_{\Pi\delta}(k)=[I^{1,1,0}_{1,g}(k)][I^{1,0,1}_{1,\delta}(k)]P(k), \tag{29}$$

such that

$$P_{\Pi\delta}(k)^{\rm t}=P^{PP}_{\Pi\delta}(k)+P^{hh}_{\Pi\delta}(k). \tag{30}$$

The calculation of galaxy-pressure power spectrum requires knowledge on the galaxy distribution within dark matter halos. Following [15], we describe the average number of galaxies per halo, $\langle N_g\rangle$ in Eq. (12), such that

$$\langle N_g\rangle=\begin{cases}\left(\dfrac{M}{M_{\rm min}}\right)^{0.6}, & M\geqslant M_{\rm min},\\ 0, & M<M_{\rm min},\end{cases} \tag{31}$$

where $M_{\rm min}$, the minimum dark matter halo mass in which a galaxy is found, is taken to be $5.3\times10^{11}h^{-1}$ $M_\odot$ for our fiducial ΛCDM cosmological model following [37]. The above relation is consistent with semianalytical models. however, we ignore scatter in the observed distribution on the mean number of galaxies per halo.

With the average number of galaxies per halo, as a function of mass, the mean number density of galaxies can be written as an integral over the PS mass function

$$\overline{n_g}=\int dM\langle N_g\rangle\frac{dn}{dM}(M,z). \tag{32}$$

In practice, the cross correlation between galaxy distribution and any other field requires the knowledge on the observable galaxy properties such as the magnitude limit, relation between luminosity and mass, etc. The same restriction arising from observing conditions can be introduced as part of the weight function that takes into account the redshift projection of galaxies.

F. Pressure bispectrum

Following [20], we can write the pressure bispectrum as

$$B^{\rm t}_\Pi=B^{\rm PPP}_\Pi+B^{\rm Phh}_\Pi+B^{\rm hhh}_\Pi, \tag{33}$$

where

$$B^{\rm PPP}_\Pi(k_1,k_2,k_3)=I^{0,3,0}_{3,ggg}(k_1,k_2,k_3), \tag{34}$$

for single halo contributions,

$$B^{\rm Phh}_\Pi(k_1,k_2,k_3)=I^{1,2,0}_{2,gg}(k_1,k_2)I^{0,1,0}_{1,g}(k_3)P(k_3)+{\rm perm.} \tag{35}$$

for double halo contributions, and

$$B_{\Pi}^{\rm hhh}(k_1,k_2,k_3)=[2J(k_1,k_2,k_3)I_{1,g}^{1,1,0}(k_3)+I_{1,g}^{2,1,0}(k_3)]\times I_{1,g}^{1,1,0}(k_1)I_{1,g}^{1,1,0}1(k_2)P(k_1)P(k_2)+\text{perm.} \tag{36}$$

for triple halo contributions. Here the 2 permutations are $k_3\leftrightarrow k_1$, k_2. Second order perturbation theory tells us that [38,39]

$$J(k_1,k_2,k_3)=1-\frac{2}{7}\Omega_m^{-2/63}+\left(\frac{k_3^2-k_1^2-k_2^2}{2k_1k_2}\right)^2\times\left[\frac{k_1^2+k_2^2}{k_3^2-k_1^2-k_2^2}+\frac{2}{7}\Omega_m^{-2/63}\right]. \tag{37}$$

In addition to the pressure bispectrum, one can also define cross-correlation bispectra such as the pressure-pressure-density or pressure-density-density. These bispectra are relevant to the calculation of non-Gaussianities present in CMB through secondary anisotropies (e.g., [40]), and it is necessary to determine the higher order moments associated with cross correlations between individual effects such as SZ and weak lensing.

G. Baryons in small overdensities

The power spectrum of baryons that trace the Jeans-scale smoothed dark matter density field can be calculated following [27] (GH), where they studied simple schemes to approximate the effect of gas pressure. One such scheme that has fractional errors on the 10% level for overdensities $\lesssim 10$ is to filter the density perturbations in the linear regime as $P_b^2=f_b^2(k/k_{\rm F})P_{\delta\delta}^2$ and treat the system as collisionless baryonic particles. Their best fit is obtained with the filter

$$f_b=\frac{1}{2}\left[e^{-x^2}+\frac{1}{(1+4x^2)^{1/4}}\right] \tag{38}$$

and [27] suggests $k_{\rm F}=34\Omega_m^{1/2}h\,{\rm Mpc}^{-1}$ as a reasonable choice for the thermal history dependent filtering scale.

For such baryons, we assume that their temperature is related to photoionization energy ($\lesssim 25$ eV). The mass fraction of baryons present in such small overdensities as a function of redshift is obtained through the numerical simulations of [1].

H. Results and discussion

In Figs. 1(a) and 1(b), we show the pressure power spectrum today ($z=0$), written such that $\Delta^2(k)=k^3P(k)/2\pi^2$ is the power per logarithmic interval in wave number. In Fig. 1(a), we show individual contributions from the single and double halo terms and a comparison to the Jeans-scale smoothed dark matter density field power spectra, both linear and nonlinear, following [27] and using [32] fitting function. Here, we have taken the electron temperature to be the virial temperature given in Eq. (7). Shown here is also the gas bias $b_{\Pi}(k)$; at large scales, $b_{\Pi}(k)\sim 3$ as $k\rightarrow 0$, consistent with numerically measured bias for gas (e.g., [13]) and analytical

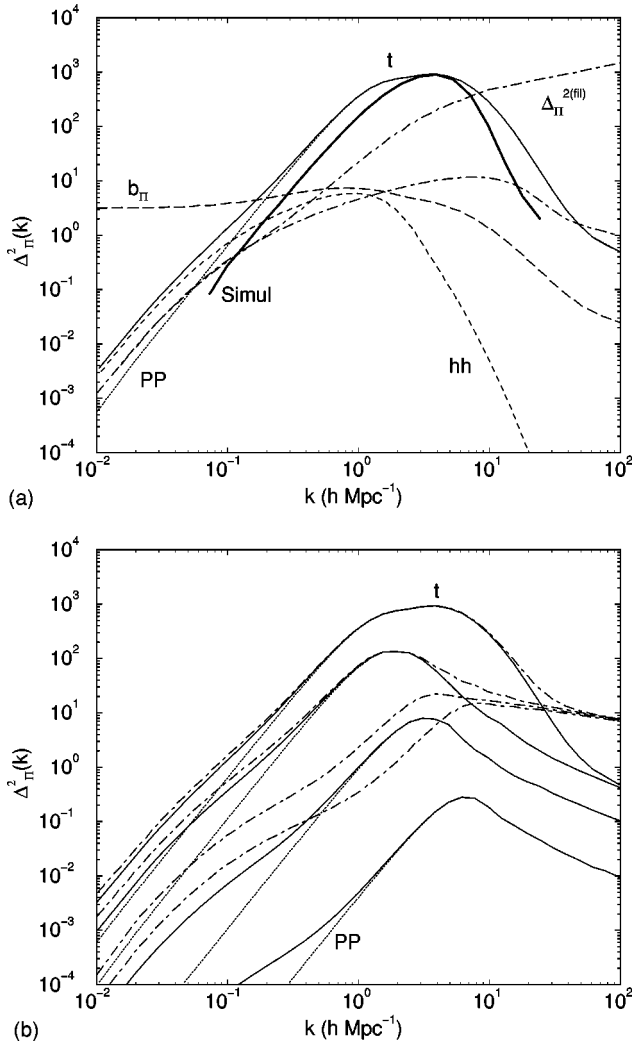

FIG. 1. Pressure power spectra with single halo (PP; dotted line), double halo (hh; dashed line) and total (t; solid line) contributions. (a) Here, we use virial temperature to describe electrons and show pressure bias, $b_\pi(k)$ (long dashed line), filtered nonlinear dark matter density power spectrum (Sec. II G) and the measured pressure power spectrum in simulations (thick solid line). (b) The variations in pressure power with maximum mass. The dot-dashed lines show the total power with a minimum electron temperature of 0.75 keV, as an attempt to reproduce power spectra under a possible preheating scenario.

estimates in [14]. The pressure power spectrum is such that at scales below $\sim$few $h\,{\rm Mpc}^{-1}$, the pressure fluctuations are suppressed relative to the dark matter power spectrum; the resulting power spectrum can also be described as a smoothed, but biased, version of the dark matter power spectrum. The scale at which smoothing enters in to the power spectrum is determined by the scale radius of the dark matter and gas profiles. Thus, the direct measurement of the pressure power spectrum, to some extent, can be used as a probe of halo profiles.

In the same figure, we also show the measured pressure power spectrum in hydrodynamical simulations by [13] for their ΛCDM model. For comparative purposes, we have appropriately corrected their pressure power spectra based on

the mean temperature of baryons as tabulated [13] since our definition of the pressure power spectrum includes the temperature. The resolution of simulations limit the accuracy of power spectrum to the range in wavenumbers of $0.2 \lesssim k \lesssim 2.0\ \mathrm{h\,Mpc^{-1}}$, and is only based on a single realization. In this range, we find that our analytical models predict more power than what is measured, while agreement is observed at scales of an $\sim$few $\mathrm{h\,Mpc^{-1}}$. The extent to which our analytical calculations agree with simulations is encouraging; this is the first time that a detailed analytical model for the pressure power spectrum has been compared with a numerically measured one. Numerical simulations with improving dynamical range and resolution will eventually test the reliability of models such as the one presented here as a useful description of the pressure fluctuations of the universe. Till then, we consider the present model as an appropriate descrption of the large scale pressure fluctuations.

In Fig. 1(b), we show the dependence of pressure power as a function of maximum mass used in the calculation with maximum mass ranging from 10^{16}, 10^{15}, 10^{14} and 10^{13} $\mathrm{M_\odot}$ from top to bottom. Here, we have shown the single halo contribution. Also shown are the total contribution to pressure power spectrum when there is an additional source of energy. Here, we have taken the minimum temperature to be ~ 0.75 keV; power spectra, in general, scale as the square of this energy if the real preheating energy is higher or lower than the one considered here. There are clear differences between the pressure power spectra with and without an additional source of energy. With increasing such additional nongravitational energy, note that b in Eq. (6) $\rightarrow 0$ such that $\rho_g(r) \rightarrow \rho_{g0}$. Thus, there is no longer a clear turn over in the pressure power spectrum since the effect of smoothing resulting from scale radius r_s is not present. The changes suggest the possibility that physical properties associated with large scale structure baryons can be probed with pressure power spectrum. In fact, the combined study of dark matter and pressure power spectra may allow a consistent determination of halo properties, and to break certain degeneracies associated with dark matter halo profile and concentration as noted in [15], while at the same time investigating presence of additional sources of energy.

In Figs. 2 and 3, we study the cross-correlation power spectra between pressure and density field and pressure and galaxy distribution, respectively. These power spectra are relevant to the study of correlations present between, say, SZ and weak gravitational lensing and SZ and galaxies, or a similar tracer of large scale structure, such as radio sources. The presence of additional source of energy clearly affects the cross-correlation power spectra, suggesting the possibility that such effects may be investigated using cross correlations between a tracer of pressure fluctuations and a tracer of matter density fluctuations.

Since the bispectrum generally scales as the square of the power spectrum, it is useful to define

$$\Delta^2_{\mathrm{eq}}(k) \equiv \frac{k^3}{2\pi^2}\sqrt{B(k,k,k)}, \tag{39}$$

which represents equilateral triangle configurations. In Fig. 4, we show the pressure bispectrum as produced by baryons present in virialized halos. Here, most of the contributions at relevant scales come from the single halo term. Given the additional dependence on temperature, and thus mass, the bispectrum is more strongly sensitive to the presence of rare and most massive halos. Thus, an increase in energy of such rare halos does not significantly change the pressure bispectrum, but such energy changes contribute when halos of mass $\lesssim 10^{14}$ $\mathrm{M_\odot}$.

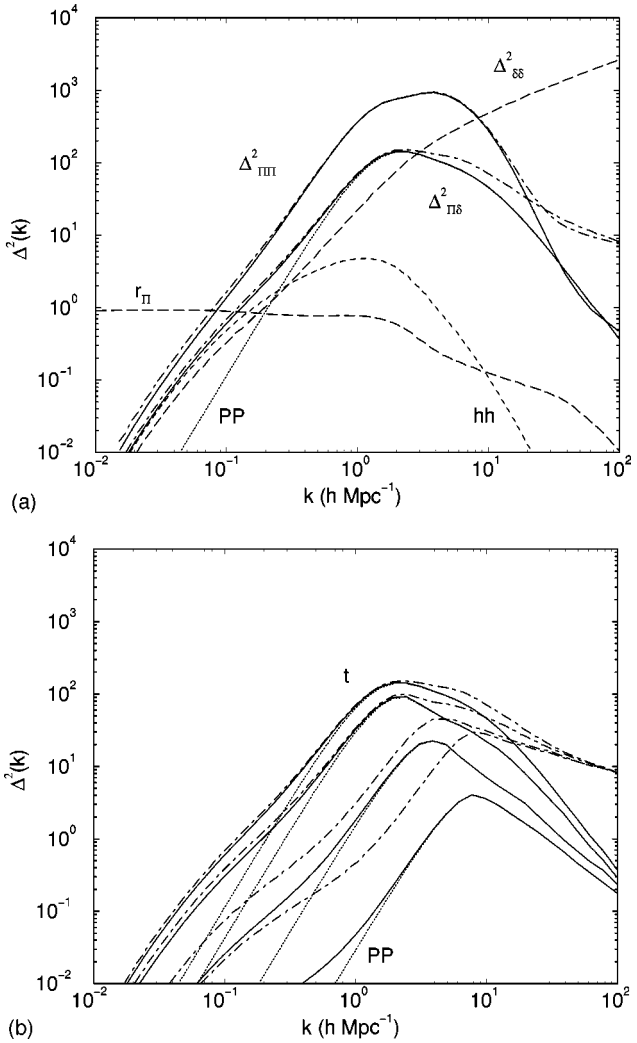

FIG. 2. Pressure-density cross-correlation power spectra. (a) Comparison of power spectra. $r_\Pi(k)$ is the correlation between dark matter and baryon distributions. (b) The variations in pressure power by changing the maximum mass considered. The figure follows Fig. 1.

III. SZ EFFECT

The temperature decrement along the line of sight due to the SZ effect can be written as the integral of pressure along the same line of sight

$$y \equiv \frac{\Delta T}{T_{\mathrm{CMB}}} = g(x)\int dr a(r)\frac{k_B\sigma_T}{m_e c^2}n_e(r)T_e(r) \tag{40}$$

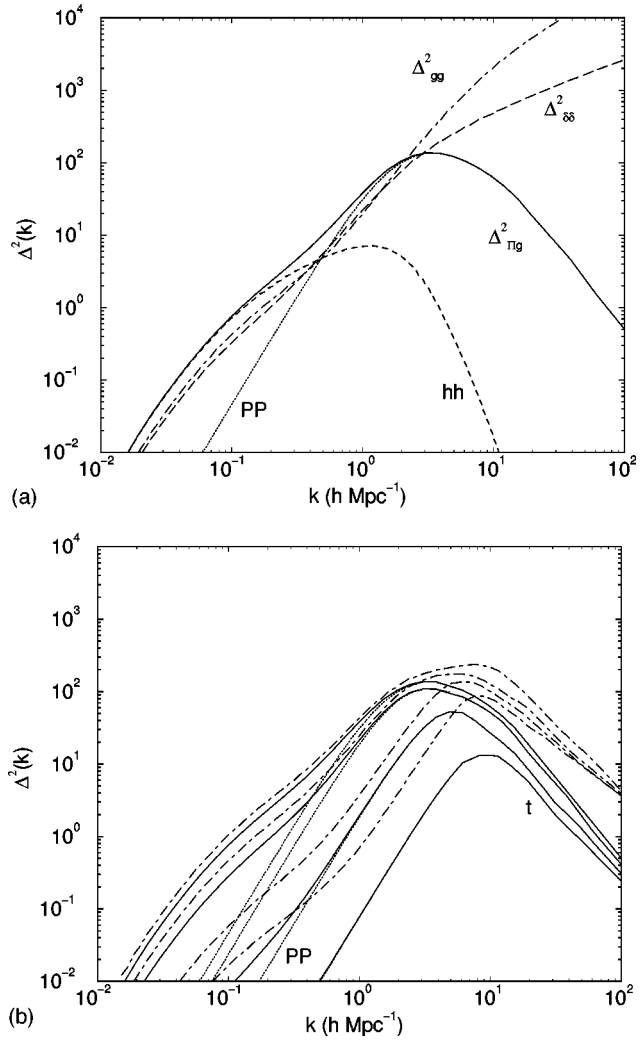

FIG. 3. Pressure-galaxy cross-correlation power spectra. (a) Comparison of pressure-gas power spectrum to the dark matter density-density and galaxy-galaxy power spectra. (b) The variations in pressure power by changing the maximum mass considered. The figure follows Fig. 1.

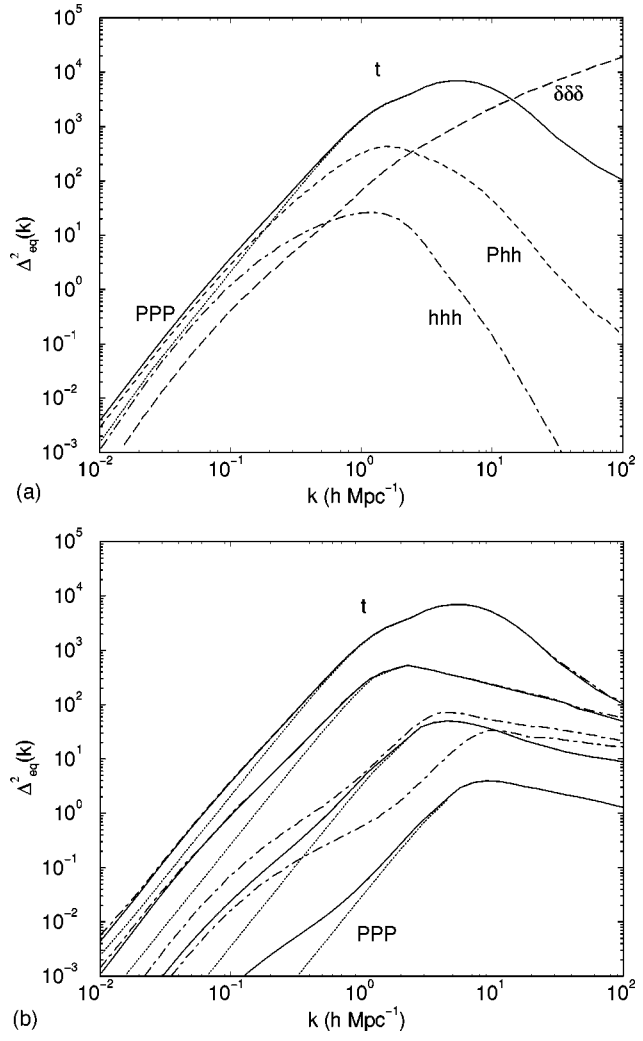

FIG. 4. Pressure bispectra. In (a), the long dashed line is the total density field bispectrum. (b) The variations in pressure power by changing the maximum mass considered. An increase in energy does not significantly increase the contribution to the bispectrum when halos with high masses are considered. This is due to the strong dependence on rare and most massive halos to the bispectrum arising from single halo term.

where σ_T is the Thomson cross section, n_e is the electron number density, r is the comoving distance, and $g(x) = x\coth(x/2) - 4$ with $x = h\nu/k_B T_{\rm CMB}$ is the spectral shape of SZ effect. At the Rayleigh-Jeans (RJ) part of the CMB, $g(x) = -2$.

The spectral dependence of the SZ effect is unique in that it can be separated from most other contributors to CMB temperature fluctuations, including the primary anisotropy itself. As discussed in Cooray *et al.* [6], the upcoming multifrequency CMB satellite and balloon-borne data, among which Planck provides the greatest information on SZ, allow the possibility for detailed studies on the SZ effect including its higher order correlations such as bispectrum and skewness. Since these observations are projected measurements of the pressure power spectrum and bispectrum along the line of sight, we now provide analytical predictions for the SZ effect based on our model for the pressure fluctuations.

A. SZ power spectrum

The angular power spectrum of the SZ effect is defined in terms of the multipole moments y_{lm} of temperature fluctuations as

$$\langle y^*_{lm} y_{l'm'} \rangle = C_l^{\rm SZ} \delta_{ll'} \delta_{mm'} . \tag{41}$$

$C_l^{\rm SZ}$ is numerically equal to the flat-sky power spectrum in the flat sky limit. The SZ power spectrum can be written as a redshift projection of the pressure power spectrum

$$C_l^{\rm SZ} = \int dr \frac{W^{\rm SZ}(r)^2}{d_A^2} P^{\rm t}_{\Pi\Pi}\left(\frac{l}{d_A}, r\right), \tag{42}$$

where d_A is the angular diameter distance. At the RJ part of the frequency spectrum, the SZ weight function is

$$W^{\rm SZ}(r) = -2\frac{k_B \sigma_T \bar{n_e}}{a(r)^2 m_e c^2}, \tag{43}$$

where $\bar{n_e}$ is the mean electron density today. In deriving Eq. (42), we have used the Limber approximation [41] by setting $k = l/d_A$ and flat-sky approximation. In previous studies (e.g., [11] and references therein), the SZ power spectrum due to massive halos has been calculated following projected y parameter of individual halos. The two approaches are essentially the same since the order in which the projection is taken does not matter, except that our approach allows us to calculate intermediate 3D properties of baryons, mainly pressure.

In Fig. 5(a), we show the SZ power spectrum due to baryons present in virialized halos compared with our previous prediction for SZ effect using a biased power spectrum for pressure fluctuations following [32] nonlinear dark matter power spectrum. As shown, most of the contributions to SZ power spectrum comes from individual massive halos, while the halo-halo correlations only contribute at a level of 10% at large angular scales. This is contrary to, say, the lensing convergence power spectrum discussed in [20], where most of the power at large angular scales is due to the halo-halo correlations. The difference can be understood by noting that the SZ effect is strongly sensitive to the most massive halos due to $T \propto M^{2/3}$ dependence in temperature and to a lesser, but somewhat related, extent that its weight function increases towards low redshifts. The lensing weight function selectively probes the large scale dark matter density power spectrum at comoving distances half to that of background sources ($z \sim 0.2$ to 0.5 when sources are at a redshift of 1), but has no extra dependence on mass. We have also shown current upper limits on the temperature fluctuations at arcminute scale angular scales where potentially the physical properties of baryons can be studies. These limits come from [42] (BIMA) and [43] (ATCA).

Also shown is the contribution to SZ effect from baryons present in overdensities $\lesssim 10$ (curve labeled GH). The SZ power spectrum here was calculated by replacing the pressure power spectrum in Eq. (42) with the unbiased Jeans-scale smoothed dark matter power spectrum following [27] and assuming a mean temperature of 25 eV for these baryons. The mass fraction of baryons present in such small overdensities were taken from numerical simulations of [1] and roughly follows $\sim 0.25(1+z)$, such that at a redshift of 3 and above all of the baryons are present in such small overdensities. The power spectrum due to such baryons are roughly three orders of magnitude lower than the power spectrum predicted for SZ effect from baryons in virialized halos, but as shown in Fig. 5(b), this level is consistent with what is predicted for SZ effect when halos with mass greater than 10^{13} $M_\odot$ is not present in observed fields.

As shown in Fig. 5(b), the lack of massive halos leads to a strong suppression of power, and halos with masses greater than 10^{15} $M_\odot$ are needed to obtain the full power spectrum. The lack of massive halos not only leads to a change in the power spectrum at large angular scales, the lack of masses also affects the contribution at small angular scales. Increasing the minimum temperature of electrons from the values determined by virial theorem to a minimum energy value of 0.75 keV significantly affects the change resulting from the lack of massive halos. In fact, with a minimum energy for baryons, the change is smaller when halos with masses less than 10^{14} $M_\odot$ are considered. At the higher end of masses, the minimum energy does not significantly affect the power spectrum; the resulting change is less than 30% compared to the power spectrum with electron temperature based on the

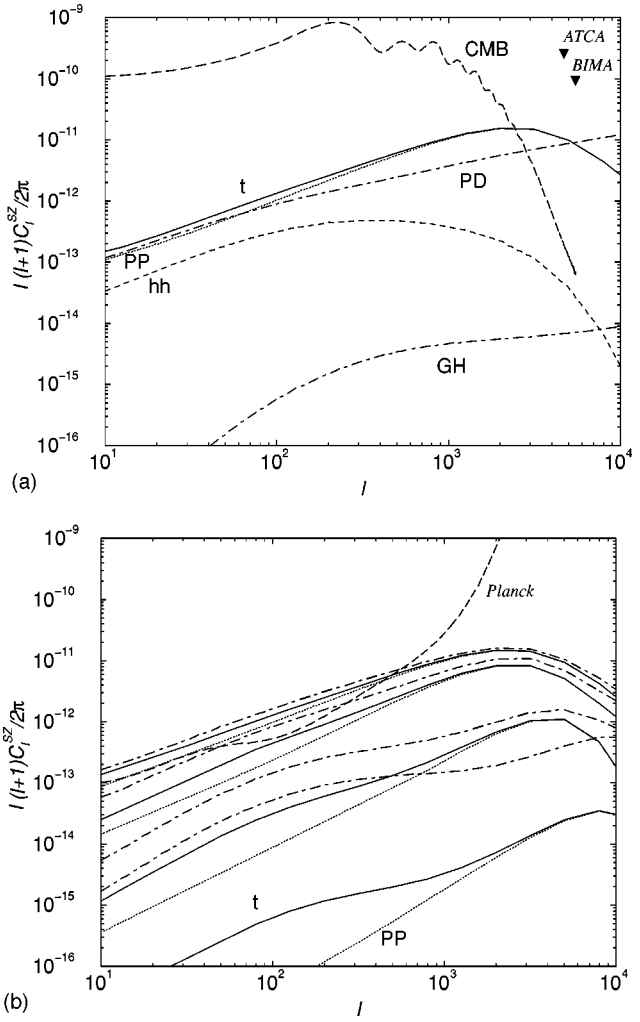

FIG. 5. SZ power spectrum. (a) The halo-halo correlations (dashed line) contribute less than 10% to the total SZ power (solid line). The signal halo terms are shown with a dotted line. We also show the SZ power spectra based on our previous prediction using a scale-independent bias model of PD nonlinear dark matter power spectrum and using the GH Jeans-smoothed unbiased power spectrum to describe baryons present in small overdensities with photoionization temperatures. For comparison, we also show the power spectrum of lensing primary anisotropies and the upper limits on temperature anisotropies at arcminute scales from BIMA and ATCA. (b) The effect of maximum mass on the power spectra, with maximum mass as in Fig. 1. The dot-dashed lines are the total SZ power when the minimum temperature is 0.75 keV. We also show the noise variance of the Planck SZ map, as has been calculated based on SZ spectral dependence and Planck detector noise. The power spectrum of SZ effect will be easily measured with Planck.

virial theorem. The variations suggest several observational possibilities, including the determination of minimum electron temperature, i.e., the energy related to preheating if it exists, by calculating the power spectrum with massive halos substratced in a wide-field SZ map such as the one that will be eventually made with Planck.

For less area surveys, such as planned interferometric observations of the wide-field SZ effect (e.g., the few square degree survey of Carlstrom *et al.* [7]), the sample variance due to lack of massive halos in observed fields can be problematic in the interpretation of the observed signal. The problem arises from the fact that massive halos which contribute to the SZ power spectrum are rare and that observations in small fields will not contain such adeqaute masses to provide the fully expected SZ signal. The dependance of SZ effect on massive halos is even problematic for numerical simulations with limited box sizes. As pointed out by [14], the measured power spectrum in their simulation varies significantly based on the considred line of sight.

The dependence of signal on massive halos is also present in other observables of large scale structure, such as weak gravitational lensing. Compared to weak lensing surveys, studied in [20] and [19], the SZ effect depends more strongly on rare halos. Most of these halos are at low redshifts, thus, surveys which avoid regions with known clusters will inherently also include an additional bias. As an example, the contribution to 1-σ detection of temperature anisotropies at arcminute scales by [42] due to SZ effect requires detailed knowledge on the distribution of halo masses in the observed fields. For a measurement of the SZ power spectrum, with a sample variance less than 20%, requires observations of a field ~ 1000 deg^2, while the same can be achieved in an area of ~ 100 deg^2 for lensing. As discussed in [20], however, the sample variance due to lack of massive and rare halos, which dominate the SZ power, does not directly imply a systematic bias as long as one uses an approach similar to the one suggested by carefully accounting for the sample variance that may be present from lack of massive halos. Such an approach requires a reliable model for the SZ effect and detailed numerical simulations will be required for such a study.

These issues can be ignored for the upcoming wide field CMB experiments, such as Planck, where the frequency coverage will allow the recovery of SZ effect over 65% of the sky not confused by galactic emissions, thereby, providing an accurate measurement of its power spectrum and higher order statistics (see [6]). Such a wide-field SZ map is also highly desirable for several reasons including the presence of adequate mass distribution of the universe such that a fair sample is considered and the possibility to use such a wide-field map for various cross-correlations purposes, such as against Sloan galaxy distribution or a wide-field weak lensing survey (see Secs. III C and III D).

B. SZ bispectrum and skewness

The angular bispectrum of the SZ effect is defined as

$$\langle y_{l_1 m_1} y_{l_2 m_2} y_{l_3 m_3}\rangle = \begin{pmatrix} l_1 & l_2 & l_3 \\ m_1 & m_2 & m_3 \end{pmatrix} B^{\rm SZ}_{l_1 l_2 l_3} \qquad (44)$$

and can be written following Limber approximation as

$$B^{\rm SZ}_{l_1 l_2 l_3} = \sqrt{\frac{(2l_1+1)(2l_2+1)(2l_3+1)}{4\pi}} \begin{pmatrix} l_1 & l_2 & l_3 \\ 0 & 0 & 0 \end{pmatrix} \times \left[\int dr \frac{[W^{\rm SZ}(r)]^3}{d_A^4} B^{\rm t}_{\rm II}\left(\frac{l_1}{d_A}, \frac{l_2}{d_A}, \frac{l_3}{d_A}; r\right)\right]. \qquad (45)$$

The more familiar flat-sky bispectrum is simply the expression in brackets [44]. The basic properties of the Wigner-3j symbol introduced above can be found in [6].

Similar to the density field bispectrum, we define

$$\Delta^2_{{\rm eq}l} = \frac{l^2}{2\pi}\sqrt{|B^{\rm SZ}_{lll}|}, \qquad (46)$$

involving equilateral triangles in l-space. The absolute value of $B^{\rm SZ}$ is considered in the above since $B^{\rm SZ} \propto g(x)^3$, which is a negative quantity at the RJ part of the frequency spectrum with $g(x) = -2$.

In Fig. 6(a), we show individual contributions $\Delta^2_{{\rm eq}l}$ with a maximum mass of 10^{16} $M_\odot$. As shown, the main contribution to bispectrum comes from individual halo term, while other terms involving correlations between halos contribute $\lesssim 10\%$. In Fig. 6(b), we show bispectrum as a function of maximum mass used in the calculation. Here, we have shown the total contribution to the bispectrum in solid lines while the total bispectrum in the presence of a minimum temperature of 0.75 keV is shown with a dot-dashed line. The bispectrum, as discussed in Sec. II H, is strongly sensitive to the single halo term due to additional mass weighing. Almost all of the contributions to the SZ bispectrum comes from the single halo term. The same dependence on mass massive rare halos decreases the effect of a temperature increase when maximum mass in $\gtrsim 10^{15}$ $M_\odot$. This is in contrast to the power spectrum, where differences are still present with an increase in temperature from virial to a minimum of 0.75 keV.

The measurement of the full bispectrum in million to billion pixel data of a wide-field SZ map as the one that will be produced with Planck can in general be difficult. In fact, there is no algorithm yet to measure the full bispectrum in such wide-field data in a reasonable time and computational requirements. Given such a possibility, it is interesting to consider a collapsed measurement of the bispectrum; real space statistics such as the third moment and skewness allow this possibility. In fact, the skewness has now been measured for the COBE data by [50], while the bispectrum measurements have only been limited to specific configurations of the bispectrum such as equilateral triangles in l-space [51]. The skewness allows an easily measurable aspect of the bispectrum and will probably be one of the first measurements of non-Gaussianity in a wide-field SZ map. The skewness can be calculated using the second, $\langle y^2(\sigma)\rangle$, and third, $\langle y^3(\sigma)\rangle$, moments of the SZ effect:

$$S_3(\sigma) = \frac{\langle y^3(\sigma)\rangle}{\langle y^2(\sigma)\rangle^2}, \qquad (47)$$

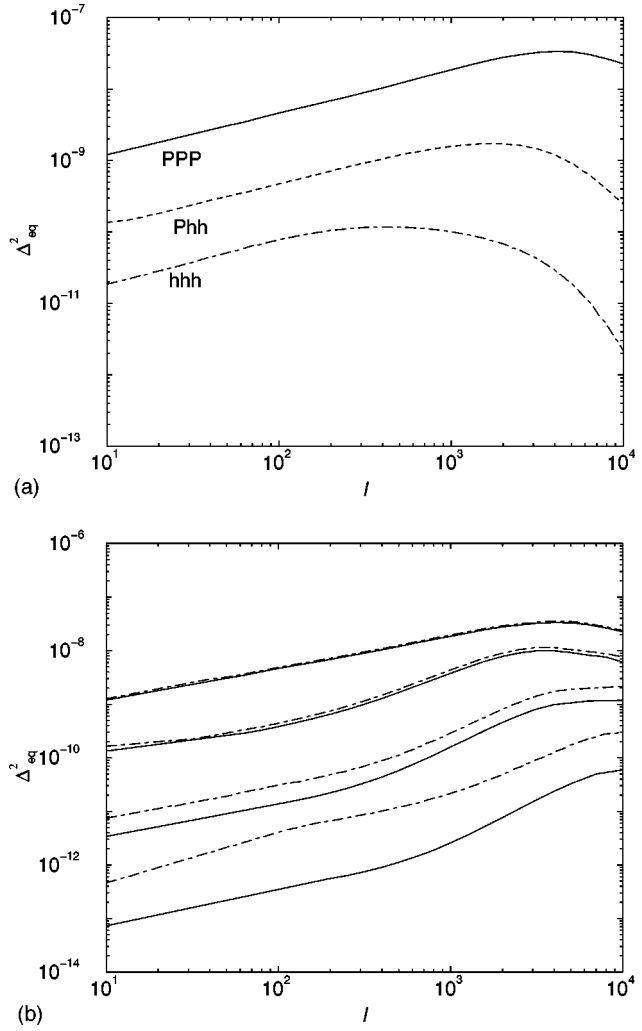

FIG. 6. SZ bispectrum. (a) The triple halo, halo-halo-halo, (dot dashed line) and double halo, Poisson-halo-halo, correlations contribute less than 10% to the total SZ bispectrum (solid line). (b) The effect of maximum mass on the bispectrum, with maximum mass as in Fig. 1. The dot-dashed lines are the total SZ bispectrum when the minimum temperature is 0.75 keV. Given the strong dependence on mass here, the increased temperature does not significantly change the bispectrum when maximum mass is greater than 10^{15} $M_\odot$.

where the two moments are

$$\langle y^3(\sigma)\rangle = \frac{1}{4\pi}\sum_{l_1 l_2 l_3}\sqrt{\frac{(2l_1+1)(2l_2+1)(2l_3+1)}{4\pi}} \times \begin{pmatrix} l_1 & l_2 & l_3 \\ 0 & 0 & 0 \end{pmatrix} B^{\rm SZ}_{l_1 l_2 l_3} W_{l_1}(\sigma) W_{l_2}(\sigma) W_{l_3}(\sigma) \tag{48}$$

and

$$\langle y^2(\sigma)\rangle = \frac{1}{4\pi}\sum_l (2l+1) C_l^{\rm SZ} W_l^2(\sigma). \tag{49}$$

In Fig. 7(a), we show the absolute value of skewness,

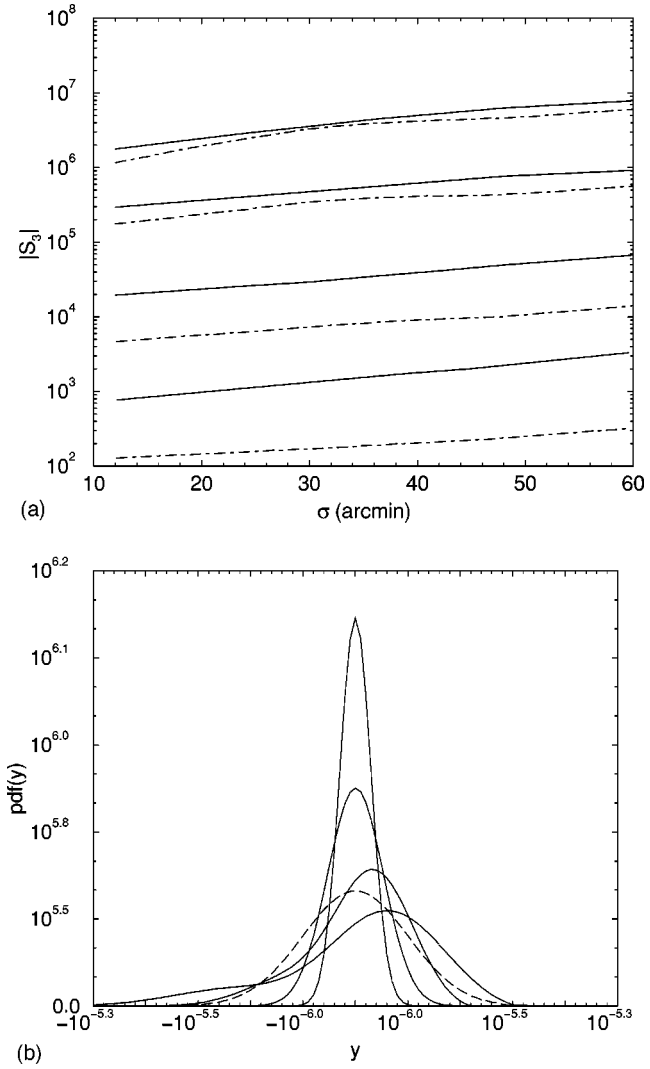

FIG. 7. (a) SZ skewness as a function of smoothing scale. The absolute value of skewness, since $S_3 \propto g(x)^{-1} < 0$ as $g(x) = -2$ at RJ part of the frequency spectrum, is shown for the virial temperature (solid lines) and minimum temperature (dot-dashed lines) models for halos as a function of maximum mass used in the calculation ranging from 10^{16} to 10^{13} $M_\odot$ from top to bottom. (b) The probability distribution function when the smoothing scale is 12 arcmin as a function of maximum mass used (solid lines; the highest peak curve is when the maximum mass is 10^{13} $M_\odot$, while with increasing non-Gaussianity as demonstrated by the departure from a Gaussian distribution, the maximum mass increases). We also show the pdf of expected Planck SZ map noise (dashed line) for smoothing at same angular scales. The non-Gaussian tail, at the negative y values beyond the pdf of Planck noise, due to massive and rare clusters will easily be detected with Planck.

$|S_3(\sigma)|$, as a function of smoothing scale σ when the maximum mass included in the calculation ranges from 10^{16} to 10^{13} $M_\odot$ (from top to bottom). The absolute value of skewness is considered since $S_3 \propto g(x)^{-1}$, which is a negative quantity at RJ part of the frequency spectrum with $g(x) = -2$. As shown, the SZ skewness is heavily dependent on the presence of most massive and rare halos. The introduction of a minimum energy of 0.75 keV leads to a decrease in

skewness, which results from the fact that the power spectrum is more affected than the bispectrum by such an increase.

Given the dependence on rare and most massive halos, the SZ effect is considerably non-Gaussian. As discussed in [35], the non-Gaussianity can be used as a useful tool for the identification and separation of most rare and massive halos from the wide-field CMB data. An optimised algorithm that utilized both the non-Gaussianity of SZ effect and its frequency dependence will be useful for constructing a catalog of SZ clusters in upcoming wide-field data. With massive clusters separated out, the remaining contribution to the SZ effect will be from halos of mass $\lesssim 10^{14}\ \mathrm{M}_{\odot}$, such as galaxy groups. In [6], we considered the contribution from such small halos as the one due to large scale structure. The extent to which such small halos contribute to the SZ power spectrum and higher order statistics clearly depends on the role of additional energy in baryons. Therefore, any measurement of the power spectrum with known massive clusters removed, can be in return used as a probe of physical properties related to baryons, mainly the extent to which preheating affects the electron temperature of low mass halos.

Instead of individual non-Gaussian statistics as skewness, one can construct the probability distribution function (pdf) using a SZ map smoothed on some scale σ. The use of pdf as a probe of cosmology was first suggested by [45] for weak gravitational lensing convergence. The same technique can be easily extended to SZ. Using the Edgeworth expansion to capture small deviations from Gaussianity, one can write the pdf of SZ effect to second order as

$$p(y)=\frac{1}{\sqrt{2\pi\langle y^2(\sigma)\rangle}}e^{-y(\sigma)^2/2\langle y^2(\sigma)\rangle}\times\left[1+\frac{1}{6}S_3(\sigma)\sqrt{\langle y(\sigma)\rangle}H_3\left(\frac{y(\sigma)}{\sqrt{\langle y^2(\sigma)\rangle}}\right)\right], \quad (50)$$

where $H_3(x)=x^3-3x$ is the third order Hermite polynomial (see [46] for details).

In Fig. 7(b), we show the pdf of SZ effect at 12 arcmin as a function of maximum mass used in the calculation. As shown, the greatest departure from non-Gaussianity occurs when the maximum mass of halos is greater than $10^{14}\ \mathrm{M}_{\odot}$. Given that we have constructed the pdf using terms only out to skewness, the presented pdfs should only be considered as approximate; with increasing non-Gaussianity behavior, the approximated pdfs are likely to depart from true distributions especially in the tails. Observationally, the pdf can be constructed easily by considering a histogram of the pixel temperature values of the SZ map. Though such a construction sounds straightforward, there are likely to be complications with the interpretation of such a pdf in the presence of instrumental noise and other foregrounds. Techniques which do not directly make a wide-field map, especially interferometric observations, will again require special techniques to construct the pdf. Therefore, the extent to which the full pdf, or such a histogram, can be used as a probe of cosmology and the accuracy to which pdfs can be constructed from upcoming wide-field CMB anisotropy data, such as Planck and planned interferometric surveys (Carlstrom, private communication), need to be investigated in detail. We leave these issues for further study.

C. SZ-weak lensing cross correlation

Similar to the SZ power spectrum, the angular power spectrum of weak lensing convergence can be defined in terms of the multipole moments κ_{lm} as

$$\langle\kappa^*_{lm}\kappa_{l'm'}\rangle=C^{\kappa}_{l}\delta_{ll'}\delta_{mm'}, \quad (51)$$

and can be written in terms of the dark matter power spectrum by [47,48]

$$C^{\kappa}_{l}=\int dr\,\frac{W^{\kappa}(r)^2}{d_A^2}P^{\mathrm{t}}_{\delta}\left(\frac{l}{d_A};r\right). \quad (52)$$

When all background sources are at a distance of r_s, the lensing weight function becomes

$$W^{\kappa}(r)=\frac{3}{2}\Omega_m\frac{H_0^2}{c^2a}\frac{d_A(r)d_A(r_s-r)}{d_A(r_s)}. \quad (53)$$

The detail properties of lensing statistics, under the dark matter halo approach, is discussed in [19] and [20].

The cross correlation between the SZ effect and weak gravitational lensing can be similarly defined in terms of the individual multipole moments as

$$\langle\kappa^*_{lm}y_{l'm'}\rangle=C^{\mathrm{SZ}-\kappa}_{l}\delta_{ll'}\delta_{mm'}. \quad (54)$$

This is now related to the dark matter-pressure power spectrum by

$$C^{\mathrm{SZ}-\kappa}_{l}=\int dr\,\frac{W^{\mathrm{SZ}}(r)W^{\kappa}(r)}{d_A^2}P^{\mathrm{t}}_{\Pi\delta}\left(\frac{l}{d_A};r\right). \quad (55)$$

Finally the cross-correlation coefficient between SZ and weak lensing is

$$C(\mathrm{SZ},\kappa)_l=\frac{C^{\mathrm{SZ}-\kappa}_{l}}{\sqrt{C^{\mathrm{SZ}}_{l}C^{\kappa}_{l}}}. \quad (56)$$

D. SZ-galaxy cross correlation

Similar to the SZ-weak lensing cross correlation, one can study the cross correlation between the galaxy distribution, which traces the large scale structure, and the SZ effect. The power spectrum of galaxy distribution can be defined terms of the multipole moments g_{lm} as

$$\langle g^*_{lm}g_{l'm'}\rangle=C^{g}_{l}\delta_{ll'}\delta_{mm'}, \quad (57)$$

and can be written as a projection of the dark matter power spectrum

$$C_l^g = \int dr \frac{W^g(r)^2}{d_A^2} P_\delta^{\rm t}\left(\frac{l}{d_A};r\right). \tag{58}$$

Here, C_l^g should be understood as the 2D Fourier transform of the galaxy correlation function, generally referred to as $w(\theta)$ in the literature. The weight function for galaxy projection involves the redshift distribution

$$W^\kappa(r) = \frac{dN}{dr} \tag{59}$$

normalized such that $\int dr(dN/dr) = 1$.

As before. the cross correlation between the SZ effect and galaxy distribution can be similarly defined in terms of the individual multipole moments as

$$\langle g_{lm}^* y_{l'm'}\rangle = C_l^{{\rm SZ}-g}\delta_{ll'}\delta_{mm'}. \tag{60}$$

This is now related to the dark matter-pressure power spectrum by

$$C_l^{{\rm SZ}-g} = \int dr \frac{W^{\rm SZ}(r)W^g(r)}{d_A^2} P_{\Pi\delta}^{\rm t}\left(\frac{l}{d_A};r\right). \tag{61}$$

Finally the cross-correlation coefficient between SZ and weak lensing is

$$C({\rm SZ},g)_l = \frac{C_l^{{\rm SZ}-\kappa}}{\sqrt{C_l^{\rm SZ}C_l^g}}. \tag{62}$$

In Fig. 8, we show the SZ-weak lensing and SZ-galaxy cross-correlation power spectra as a function of maximum mass used in the calculation, while the correlation coefficients are shown in Fig. 9. In order to describe the galaxy distribution, we have considered a survey at low redshifts, similar to the Sloan Digital Sky Survey (SDSS).[1] Such a low redshift tracer is desirable since contributions to SZ effect primarily comes from large scale structures at redshifts <1. Here, we have assumed the redshift distribution of Sloan galaxies follow $dN/dz \propto z^2 \exp[(-z/z_c)^{3/2}]$ with a mean redshift z_m, of 0.2 ($z_c \sim 1.412 z_m$). For SZ-weak lensing, the cross correlation is such that SZ and lensing traces each other out to angular scales of ~ 1000 when most massive and rarest halos are involved with a decrease in cross correlation between the two at small angular scales. For SZ-galaxy cross correlation, there is additional correlation at large angular scales, when compared to lensing, while the correlation is suppressed at small angular scales. The decrease at small angular scales is due to the fact that small halos that contribute to SZ and lensing do not necessarily contribute to the galaxy power spectrum. With an increase in additional energy for halos, the cross correlation increases by few percent, however, this small increase unlikely to be determined accurately through observations. The correlation is sensitive to the redshift distribution of galaxies, which depends mostly on the selection criteria imposed by observations. The selection function of weak lensing can be considered well understood, however, a straightforward interpretation of any observed SZ-galaxy cross correlation will require a clear understanding of observable related to galaxy distribution.

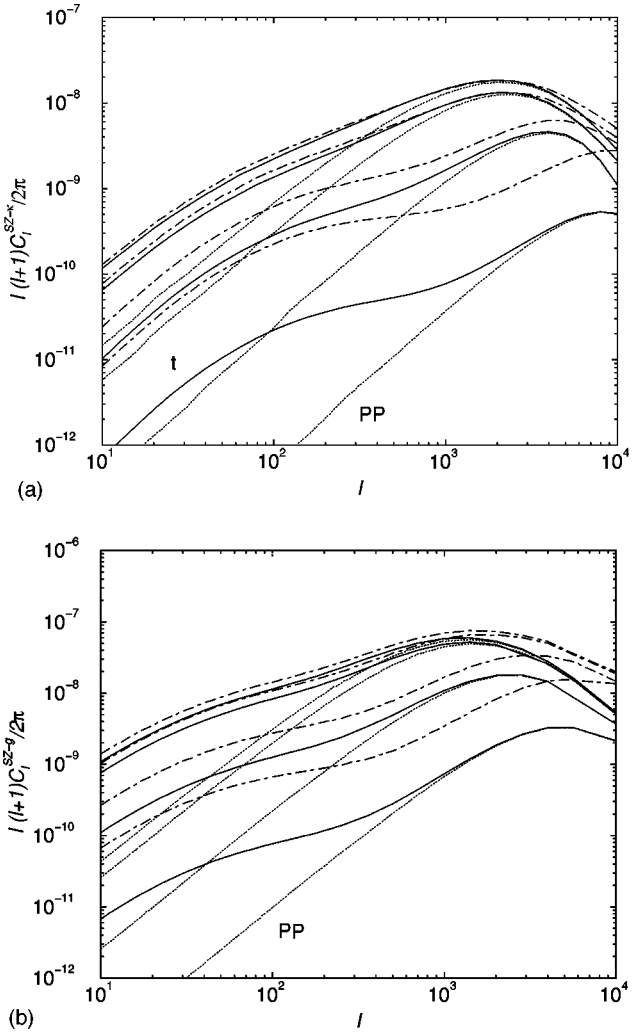

FIG. 8. SZ-weak lensing cross-correlation (a) and SZ-galaxy cross-correlation (b) power spectra as a function of maximum mass, with mass cut off following Fig. 1. The additional minimum energy, shown with a dot-dashed line, leads to an increase in the correlated power.

The SZ-SZ, lensing-lensing and SZ-lensing power spectra dependence differ on the bias and correlation parameters. Since the bias and correlation are scale and redshift dependent, the measurement of these power spectra, which are projected along the redshift distributions, do not allow a direct probe of these quantities. A useful approach would be to consider the inversion of these power spectra in redshift bins by considering the measured lensing-lensing and SZ-lensing power spectra as a function of redshift. Note that the SZ-SZ power spectrum cannot be easily separated in redshift space as we do not have the ability to separate individual redshift contributions, unlike say in lensing, where one can use the

[1]http://www.sdss.org

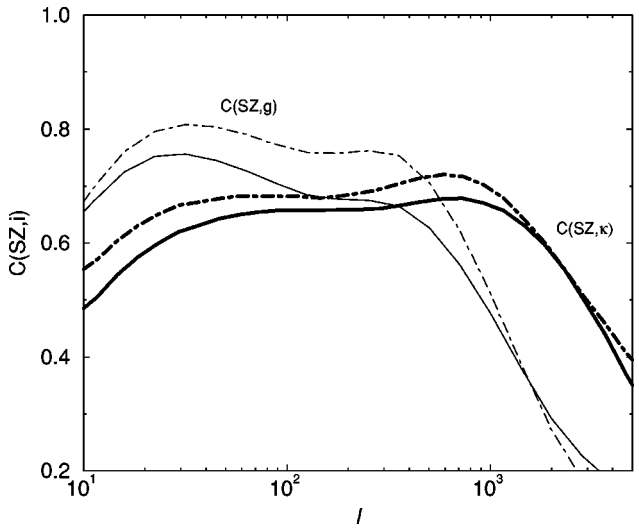

FIG. 9. The cross-correlation coefficient for SZ-weak lensing (thick lines) and SZ-galaxy (thin lines) with (solid line) and without additional energy (dashed line). In general, when the maximum mass is greater than 10^{14} $M_{\odot}$, SZ and galaxy correlate less than SZ-weak lensing at small angular scales, while the opposite is present at large angular scales. Introduction of additional energy increases the correlation by not more than a few percent; such an increase is insignificant to be determined observationally using the SZ-lensing and SZ-galaxy cross correlations, however, SZ power spectrum and skewness allow a determination as these values are significantly affected.

redshifts of background sources to construct convergence as a function of redshift. With adequate signal-to-noise from wide-field surveys, it is likely that such an approach will allow studies to be carried out on the extent to which temperature weight baryons trace the dark matter and their correlation properties.

Similarly, as studied in [49], the cross correlation of SZ against galaxy data, as a function of redshift, is expected to provide information on the properties of clustering of galaxies with respect to the temperature weighted baryon field represented by SZ effect. Such a cross correlation will help understand the extent to which hot-warm gas is present in the outskirts of individual galaxies. With individual sets of SZ, weak lensing and galaxy maps, it is likely that a tremendous amount of information on physical properties associated with dark matter, baryon and galaxy distribution will be obtained through both a comparison of individual power spectra and higher order moments and cross correlations and higher order moments associated with such cross correlations. We hope to study some of these possibilities in detail in future studies.

IV. SUMMARY AND CONCLUSIONS

Using an extension of the dark matter halo approach, we have presented an efficient method to calculate the large scale structure pressure power spectrum and its high order moments, such as bispectrum. We have divided the contribution to large scale pressure power spectrum based on the overdensities in which contributing baryons are present with (1) baryons present in virialized halos with overdensities greater than ~ 200 and in hydrostatic equilibrium with the density field of such halos, (2) photoionized baryons in overdensities less than ~ 10 and which trace the Jeans-scale smoothed dark matter density field, and (3) baryons present in the mid overdensity regime which are likely to be undergoing collapse and shock heating.

Our approach allows us to calculate not only 2D statistics such as the projected pressure power spectrum, or the SZ effect, which will be observed, but also the 3D statistics that can be directly compared to predictions based on numerical simulations. We have performed such a comparison to recently published numerical simulations by [13] and found good agreement between our analytical calculations and their simulations. The current simulations are limited to a handful of realizations and limited dynamical range and resoltion. With improving resolution and accuracy, analytical models such as the one presented here will be tested in detail against numerical calculations. Analytical calculations, aided by numerical simulations, will eventually allow detailed studies of large scale baryon distribution using observations such as the wide-field SZ effect.

The projected pressure power spectrum along the line of sight, provides a direct calculation of the large scale structure SZ effect and its higher order correlations. In the absence of massive and rare halos, we have suggested that baryons present in small overdensities provide a lower limit to any contribution to SZ effect. The extent to which baryons present in overdensities between 10 and 200 contribute to the correlations in large scale pressure and, from it, the SZ effect, requires additional studies, preferably with numerical simulations. Presently, our understanding of the role of preheating and its effect on baryons will also be another challenge as the SZ observations will clearly depend on such additional energy contributions to large scale baryon distribution. We have suggested the possibility of using SZ power spectrum and higher order correlations, such as the SZ skewness, as a probe of preheating. Such a study will require a wide-field SZ map and this task will be completed with Planck observations. The unique frequency dependence of the SZ effect, together with its non-Gaussian behavior, will allow the construction of a reliable SZ cluster catalog which will aid in cosmological studies of structure formation.

Our approach allows one to study possible systematic effects that may be present in upcoming SZ observations of small area fields due to the presence or absence of rare massive halos in such fields that will be observed. We have shown that the SZ effect as well as its non-Gaussian properties are mainly due to the most massive and rarest virialized halos in the universe. The lack of massive halos in observed SZ fields can introduce a systematic bias in the power spectrum, but the sample variance introduced by the lack of such masses, can be easily corrected based on the prior knowledge of mass distribution of observed fields. Due to additional mass dependence through temperature, the effect of mass is

such that the SZ effect is more dependent on the rare halos than weak gravitational lensing convergence. The same SZ halos also contribute to lensing convergence and the cross correlation between SZ and lensing can be used as a probe of clustering properties between density and temperature weighted baryon fields. Given the great potential to study baryon distribution using SZ, various issues suggested here involving such correlations merit further study.

ACKNOWLEDGMENTS

The author greatly thanks Wayne Hu for useful discussions and helpful suggestions that led to the calculations presented in this paper. We also acknowledge useful discussions with Gil Holder, Lloyd Knox and Joe Mohr and thank Alexandre Refregier, Ue-Li Pen and their collaborators for providing results from numerical simulation presented in [13].

[1] R. Cen and J.P. Ostriker, Astrophys. J. **514**, 1 (1999).
[2] M. Fukugita, C.J. Hogan, and P.J.E. Peebles, Astrophys. J. **503**, 518 (1998).
[3] M. Pierre, G. Bryan, and R. Gastaud, Astron. Astrophys. **356**, 403 (2000).
[4] T.M. Tripp, B.D. Savage, and E.B. Jenkins, Astrophys. J. Lett. **534**, L1 (2000).
[5] R.A. Sunyaev and Ya.B. Zel'dovich, Mon. Not. R. Astron. Soc. **190**, 413 (1980).
[6] A. Cooray, W. Hu, and M. Tegmark, astro-ph/0002238.
[7] J.E. Carlstrom, M. Joy, and L. Grego, Astrophys. J. Lett. **456**, L75 (1996).
[8] M. Jones *et al.*, Nature (London) **365**, 320 (1993).
[9] W.H. Press and P. Schechter, Astrophys. J. **187**, 425 (1974).
[10] S. Cole and N. Kaiser, Mon. Not. R. Astron. Soc. **233**, 637 (1988).
[11] E. Komatsu and T. Kitayama, Astrophys. J. Lett. **526**, L1 (1999).
[12] A.C. da Silva, D. Barbosa, A.R. Liddle, and P.A. Thomas, astro-ph/9907224.
[13] A. Refregier, E. Komatsu, D.N. Spergel, and U.-L. Pen, Phys. Rev. D **61**, 123001 (2000).
[14] U. Seljak, J. Burwell, and U.-L. Pen, Phys. Rev. D (to be published), astro-ph/001120.
[15] U. Seljak, astro-ph/0001493.
[16] C.-P. Ma and J.N. Fry, astro-ph/0003343.
[17] R. Scoccimarro, R. Sheth, L. Hui, and B. Jain (in preparation).
[18] R.J. Scherrer and E. Bertschinger, Astrophys. J. **381**, 349 (1991).
[19] A. Cooray, W. Hu, and J. Miralda-Escudé, Astrophys. J. Lett. **535**, L9 (2000).
[20] A. Cooray and W. Hu, astro-ph/0004151.
[21] J. Navarro, C. Frenk, and S.D.M. White, Astrophys. J. **462**, 563 (1996).
[22] H.J. Mo, Y.P. Jing, and S.D.M. White, Mon. Not. R. Astron. Soc. **284**, 189 (1997).
[23] J.J. Mohr and A.E. Evrard, Astrophys. J. **491**, 38 (1997).
[24] U.-L. Pen, Astrophys. J. **510**, 1 (1999).
[25] L.P. David, C. Jones, and W. Forman, Astrophys. J. **445**, 578 (1995).
[26] A. Renzini, Astrophys. J. **488**, 35 (1997).
[27] N.Y. Gnedin and L. Hui, Mon. Not. R. Astron. Soc. **296**, 44 (1998).
[28] P.T.P. Viana and A.R. Liddle, Mon. Not. R. Astron. Soc. **303**, 535 (1999).
[29] E.F. Bunn and M. White, Astrophys. J. **480**, 6 (1997).
[30] D.J. Eisenstein and W. Hu, Astrophys. J. **511**, 5 (1999).
[31] J.P. Henry, astro-ph/0002365.
[32] J.A. Peacock and S.J. Dodds, Mon. Not. R. Astron. Soc. **280**, L19 (1996).
[33] N. Makino, S. Sasaki, and Y. Suto, Astrophys. J. **497**, 555 (1998).
[34] Y. Suto, S. Sasaki, and N. Makino, Astrophys. J. **509**, 544 (1998).
[35] N. Aghanim and O. Forni, Astron. Astrophys. **347**, 409 (1999).
[36] M. Tegmark and P.J.E. Peebles, Astrophys. J. **500**, 79 (1998).
[37] A.J. Benson, S. Cole, C.S. Frenk, C.M. Baugh, and C.G. Lacey, astro-ph/9903343.
[38] J.N. Fry, Astrophys. J. **279**, 499 (1984).
[39] M. Kamionkowski and A. Buchalter, Astrophys. J. **514**, 7 (1999).
[40] A. Cooray and W. Hu, Astrophys. J. **534**, 533 (2000).
[41] D. Limber, Astrophys. J. **119**, 655 (1954).
[42] W.L. Holzapfel, J.E. Carlstrom, L. Grego, G. Holder, M. Joy, and E.D. Reese, Astrophys. J. **533**, 38 (2000).
[43] R. Subrahmanyan, M.J. Kesteven, R.D. Ekers, M. Sinclair, and J. Silk, astro-ph/0002467.
[44] W. Hu, Phys. Rev. D **62**, 043007 (2000).
[45] B. Jain and L. van Waerbeke, astro-ph/9910459.
[46] R. Juszkiewicz, D.H. Weinberg, P. Amsterdamski, M. Chodorowski, and F. Bouchet, Astrophys. J. **442**, 39 (1995).
[47] N. Kaiser, Astrophys. J. **388**, 286 (1992).
[48] N. Kaiser, Astrophys. J. **498**, 26 (1998).
[49] H.V. Peiris and D.N. Spergel, astro-ph/0001393.
[50] C.R. Contaldi, P.G. Ferreira, J. Magueijo, and K.M. Górski, Astrophys. J. **534**, 25 (2000).
[51] P.G. Ferreira, J. Magueijo, and K.M. Gorksi, Astrophys. J. **503**, 1 (1998).